Journal of Zhejiang University-SCIENCE B (Biomedicine & Biotechnology)
ISSN 1673-1581 (Print); ISSN 1862-1783 (Online)
www.jzus.zju.edu.cn; www.springerlink.com
E-mail: jzus@zju.edu.cn

Effects of calcium-binding sites in the S2–S3 loop on human and *Nematostella vectensis* TRPM2 channel gating processes*

Yu-huan LUO[1,2,3], Xia-fei YU[1], Cheng MA[4], Fan YANG[1], Wei YANG[†‡1,5]

[1]*Department of Biophysics, Institute of Neuroscience, NHC and CAMS Key Laboratory of Medical Neurobiology, School of Medicine, Zhejiang University, Hangzhou 310058, China*

[2]*Department of Pediatric, Affiliated Hangzhou First People's Hospital, Zhejiang University School of Medicine, Hangzhou 310006, China*

[3]*Translational Medicine Research Center, Key Laboratory of Clinical Cancer Pharmacology and Toxicology Research of Zhejiang Province, Affiliated Hangzhou First People's Hospital, Zhejiang University School of Medicine, Hangzhou 310006, China*

[4]*Co-facility Center, Zhejiang University School of Medicine, Hangzhou 310058, China*

[5]*Department of Neurosurgery, the First Affiliated Hospital, School of Medicine, Zhejiang University, Hangzhou 310003, China*

[†]E-mail: yangwei@zju.edu.cn

Received Aug. 9, 2019; Revision accepted Oct. 9, 2019; Crosschecked Oct. 23, 2019

Abstract: As a crucial signaling molecule, calcium plays a critical role in many physiological and pathological processes by regulating ion channel activity. Recently, one study resolved the structure of the transient receptor potential melastatin 2 (TRPM2) channel from *Nematostella vectensis* (nvTRPM2). This identified a calcium-binding site in the S2–S3 loop, while its effect on channel gating remains unclear. Here, we investigated the role of this calcium-binding site in both nvTRPM2 and human TRPM2 (hTRPM2) by mutagenesis and patch-clamp recording. Unlike hTRPM2, nvTRPM2 cannot be activated by calcium alone. Moreover, the inactivation rate of nvTRPM2 was decreased as intracellular calcium concentration was increased. In addition, our results showed that the four key residues in the calcium-binding site of S2–S3 loop have similar effects on the gating processes of nvTRPM2 and hTRPM2. Among them, the mutations at negatively charged residues (glutamate and aspartate) substantially decreased the currents of nvTRPM2 and hTRPM2. This suggests that these sites are essential for calcium-dependent channel gating. For the charge-neutralizing residues (glutamine and asparagine) in the calcium-binding site, our data showed that glutamine mutating to alanine or glutamate did not affect the channel activity, but glutamine mutating to lysine caused loss of function. Asparagine mutating to aspartate still remained functional, while asparagine mutating to alanine or lysine led to little channel activity. These results suggest that the side chain of glutamine has a less contribution to channel gating than does asparagine. However, our data indicated that both glutamine mutating to alanine or glutamate and asparagine mutating to aspartate accelerated the channel inactivation rate, suggesting that the calcium-binding site in the S2–S3 loop is important for calcium-dependent channel inactivation. Taken together, our results uncovered the effect of four key residues in the S2–S3 loop of TRPM2 on the TRPM2 gating process.

Key words: TRPM2; Calcium-binding site; S2–S3 loop; Channel activation; Channel inactivation
https://doi.org/10.1631/jzus.B1900477 **CLC number:** Q615

1 Introduction

As a calcium permeable, non-selective cation channel, transient receptor potential melastatin 2 (TRPM2) channel serves as an oxidative stress sensor, and is involved in many physiological and pathological processes by regulating the calcium balance

‡ Corresponding author
* Project supported by the National Natural Science Foundation of China (Nos. 81371302, 81571127, and 31872796), the National Basic Research Program (973) of China (No. 2014CB910300), the National Major New Drugs Innovation and Development (No. 2018ZX 09711001-004-005), and the Zhejiang Provincial Natural Science Foundation of China (Nos. LR16H090001 and LY19B020013)
ORCID: Yu-huan LUO, https://orcid.org/0000-0002-6334-6151

(Jiang et al., 2010). It is well known that TRPM2 is widely expressed in various tissue cells such as neurons, immune cells, and so on (Gao et al., 2014; Kheradpezhouh et al., 2014; Miller et al., 2014; Yonezawa et al., 2016; Huang et al., 2017; Li and Jiang, 2018). As a tetramer, the TRPM2 channel contains four subunits, and each subunit has the six transmembrane segments (S1–S6), with intracellular N and C termini (Nagamine et al., 1998; Perraud et al., 2001).

Accumulating evidence has indicated that gating mechanisms of the TRPM2 are very complex. For example, TRPM2 activation not only needs ligands such as adenosine diphosphate ribose (ADPR) and cyclic ADPR (cADPR), but also requires intracellular calcium interacting with its N-terminus. In addition, calcium activates TRPM2 and its spliced isoforms by itself (Lange et al., 2008; Du et al., 2009; Tóth and Csanády, 2010). Inactivation is another important process during channel gating. Our previous studies indicated that TRPM2 can be inactivated by protons (Yang et al., 2010) and metal ions outside the membrane, such as Zn^{2+} (Yang et al., 2011) and Cu^{2+} (Yu et al., 2014). The mutation of TRPM2 (P1018L) also induces channel inactivation (Hermosura et al., 2008).

Recently, several studies have identified the key sites involved in calcium-mediated TRPM2 activation. There is an IQ-like motif in the N-terminus of TRPM2, which is critical for channel activation by interacting with calmodulin. In addition, our previous study identified a novel EF-loop in the TRPM homology domain of TRPM2 important for the calcium-activated TRPM2 channel (Luo et al., 2018). Interestingly, a recent study showed that there is a calcium-binding site in the S2–S3 loop of *Nematostella vectensis* TRPM2 (nvTRPM2), while the role of this site on the channel gating process is unknown (Zhang et al., 2018).

As a distantly related orthologue, the property of nvTRPM2 channel is different from human TRPM2 (hTRPM2). For example, the NUDT9 homology (NUDT9-H) domain in nvTRPM2 conserved the enzyme activity for catalyzing ADPR (Kühn et al., 2017). Although recent studies identified a calcium-binding site in the S2–S3 loop of nvTRPM2 that may be involved in the calcium-dependent regulation of the nvTRPM2 channel activity (Zhang et al., 2018), the underlying mechanism is still unclear. Moreover, a recent study claimed that there is a calcium-binding site in the S2–S3 loop of hTRPM2 (Wang et al., 2018), but the effect of this site on the channel gating is also unknown.

In this study, we tried to determine the role of the calcium-binding site in the S2–S3 loop of both hTRPM2 and nvTRPM2 on the channel gating process by combining mutagenesis with electrophysiological recordings in mammalian human embryonic kidney 293T (HEK293T) cells. By substituting the different property residues for the individual residue in the four key residues in the calcium-binding site, we examined the contribution of these residues to the TRPM2 gating process. Our data indicate the importance of the calcium-binding site in the S2–S3 loop for the calcium-dependent TRPM2 channel gating regulation.

2 Materials and methods

2.1 Cells, clones, and transfection

Cell culture, mutagenesis, and transfection experiments were performed as previously described (Luo et al., 2018). Briefly, HEK293T cells were maintained in Dulbecco's modified Eagle medium (DMEM), to which is added 10% fetal bovine serum (FBS; Gibco, USA). Site-directed mutagenesis was carried out for all the mutant constructions, and verified by sequencing. hTRPM2, nvTRPM2, or their mutants were transiently transfected into HEK293T cells using Lipofectamine 2000 (Thermo Fisher Scientific, USA). The transfected cells were subsequently seeded on glass coverslips at 24 h after the transfection, and used for electrophysiological recording tests 12 h later. Chemicals and reagents used were purchased from Sigma Aldrich (MO, USA) unless otherwise indicated.

2.2 Patch clamp recording

Electrophysiological recording experiments were performed as previous described (Luo et al., 2018). Briefly, the data were acquired at room temperature using an EPC10 amplifier (HEKA Electronic, Lambrecht, Germany) and PatchMaster software. The resistance of patch electrodes was 3–5 MΩ when filled with internal solutions by pulling from borosilicate glass (Sutter Instrument Co., Novato, CA, USA). All the currents were acquired at 20 kHz and filtered offline at 50 Hz. The recording protocol uses

voltage ramps from −100 to +100 mV within 500 ms given every 5 s. The amplitudes of currents at −60 mV are denoted by circles in the Figures. We used the maximal current amplitudes (pA) divided by cell capacitance (pF) as current density (pA/pF) for data analysis.

As our previous study described (Luo et al., 2018), the intracellular solution of high calcium in Fig. 1 contained (in mmol/L): 75 NaCl, 50 $CaCl_2$, 1 $MgCl_2$, and 10 N-2-hydroxyethylpiperazine-N'-2-ethanesulfonic acid (HEPES), pH 7.4, adjusted with NaOH. The internal pipette solution for the cells which were successfully transfected with hTRPM2 or its different mutants contained (in mmol/L): 147 NaCl, 1 $MgCl_2$, 10 HEPES, and 0.5 ADPR, pH 7.4. The free Ca^{2+} was adjusted to different levels (calculated by Maxchelator) using indicated concentration of ethylene glycol tetraacetic acid (EGTA) in Fig. 1 and 0.05 mmol/L EGTA in Figs. 4, 6, and 7. The standard intracellular solution for the cells transfected with nvTRPM2 or its different mutants contained (in mmol/L): 145 CsCl, 8 NaCl, 2 $MgCl_2$, 10 HEPES, and 0.5 ADPR, pH 7.2. Free Ca^{2+} was chelated to different levels using the indicated concentration of EGTA in Fig. 1 and 10 mmol/L EGTA in Figs. 2, 6, and 7. The standard extracellular solution for cells expressing hTRPM2 and its mutants contained (in mmol/L): 147 NaCl, 2 KCl, 2 $CaCl_2$, 1 $MgCl_2$, 13 glucose, and 10 HEPES, pH 7.4. The standard extracellular solution for cells expressing nvTRPM2 and its mutants contained (in mmol/L): 140 NaCl, 5 KCl, 1.2 $CaCl_2$, 1.2 $MgCl_2$, and 10 HEPES, pH 7.4. After the currents became stable, 20 μmol/L *N*-(pamylcinnamoyl) anthranilic acid (ACA) (Sigma Aldrich) was used to inhibit TRPM2 currents. The change time of bath solution is about 100 ms controlled by RSC-200 (Bio-logic Science Instruments, Grenoble, France). We only used cells for data analysis whose currents were less than 200 pA after the inhibition of ACA.

2.3 Biotinylation assay and western blot

Biotinylation experiments were carried out as previously described (Yu et al., 2017; Luo et al., 2018). Rabbit anti-TRPM2 (1:1000 dilution; Abcam, UK) was used as primary antibody and goat anti-rabbit IgG-horseradish peroxidase (HRP) (1:10 000 dilution; Thermo Fisher Scientific, USA) was used as secondary antibody. Enhanced chemiluminescence (ECL; Thermo Fisher Scientific, USA) was used to detect the signal, and the images were acquired by a Fuji LAS-3000 Imaging System (FUJIFILM, Tokyo, Japan).

2.4 Statistical analysis

All of the electrophysiological data were acquireed by PatchMaster (HEKA) and Igor Pro (Wave Metrics, OR, USA). The electrophysiological data are presented as mean±standard error of the mean (SEM). and Origin software is used for curve fitting. Statistical analysis was performed using Student's *t*-test ($P<0.05$ designated as significant).

3 Results

3.1 Roles of calcium in the gating process of hTRPM2 and nvTRPM2

It has been reported that calcium can activate hTRPM2 directly by itself (Du et al., 2009; Luo et al., 2018), but whether it can open nvTRPM2 alone remains unknown. We transfected hTRPM2 or nvTRPM2 channel into HEK293T cells, and detected whether 50 mmol/L calcium induces the current by using whole-cell recordings. Consistent with our previous studies (Yu et al., 2017; Luo et al., 2018), 50 mmol/L calcium activated hTRPM2 current, which was inhibited by 20 μmol/L ACA (Figs. 1a and 1b). However, nvTRPM2 failed to be activated by 50 mmol/L calcium alone (Figs. 1a and 1b).

In order to further address the effect of endogenous calcium on hTRPM2 and nvTRPM2 channels, we gradually chelated the intracellular calcium by adding 10, 1, or 0.05 mmol/L EGTA into the intracellular solution, separately. Although 500 μmol/L ADPR fully activated the hTRPM2 channel in both the 0.05 and 1 mmol/L EGTA conditions, the hTRPM2 channel failed to respond to 500 μmol/L ADPR in the 10 mmol/L EGTA condition (Figs. 1c and 1e). We noted that the open probability of hTRPM2 by 1 mmol/L EGTA (33.3%) is less than that of hTRPM2 by 0.05 mmol/L EGTA (100.0%). Our results confirmed that the hTRPM2 activation is dependent on intracellular calcium.

Since a previous study reported that nvTRPM2 has a rapid inactivation (Kühn et al., 2015), we also examined the response of nvTRPM2 in different intracellular calcium conditions. Unlike hTRPM2, our data showed that the nvTRPM2 current induced by

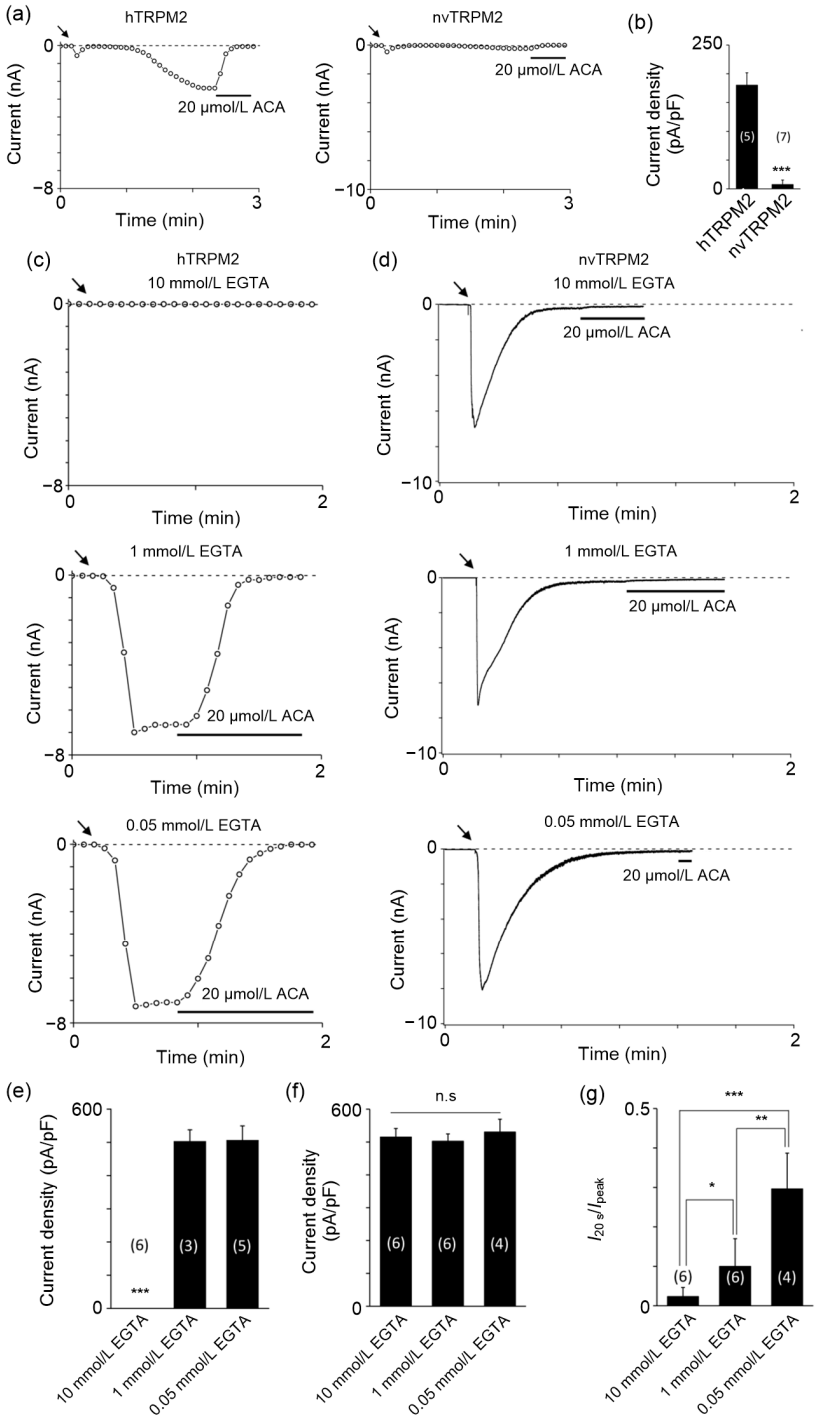

Fig. 1 Effects of intracellular calcium on the gating property of hTRPM2 and nvTRPM2

(a) Representative whole-cell recordings induced by 50 mmol/L Ca^{2+} from HEK293T cells expressing human transient receptor potential melastatin 2 (hTRPM2; left panel) and *Nematostella vectensis* TRPM2 (nvTRPM2; right panel). The arrow in each panel indicates the time point at which whole-cell configuration was established. The black lines represent application of 20 μmol/L *N*-(pamylcinnamoyl) anthranilic acid (ACA). (b) Summary of the current density in (a). (c, d) Representative whole-cell recordings induced by 500 μmol/L adenosine diphosphate ribose (ADPR) with 10 mmol/L ethylene glycol tetraacetic acid (EGTA) (top panel), 1 mmol/L EGTA (middle panel), and 0.05 mmol/L EGTA (bottom panel), from HEK293T cells expressing hTRPM2 (c) and nvTRPM2 (d). (e, f) Summary of the current density in (c, d). (g) Summary of the inactivation rate of nvTRPM2, expressed as the percentage of the residual currents 20 s after the maximal current amplitudes from the peak currents. Data are expressed as mean±standard error of the mean (SEM). The numbers of cells examined in each case are indicated in parentheses. * P<0.05, ** P<0.01, *** P<0.001, compared with different concentrations of EGTA treatment groups. n.s.: not significant

500 μmol/L ADPR is independent of the concentration of EGTA in cytoplasm (Figs. 1d and 1f). However, we noticed that the inactivation rate of nvTRPM2 in 10 mmol/L EGTA was less than that of nvTRPM2 in 0.05 mmol/L EGTA (Fig. 1g). This suggests that the inactivation process of nvTRPM2 is dependent on intracellular calcium instead of activation.

3.2 Role of the key residues within the calcium-binding site in S2–S3 loop of nvTRPM2

It is pointed out that calcium is coordinated in a pentacovalent geometry formed by the side chains of E893, Q896, N918, and D921 in nvTRPM2, among which E893 provides two coordinate bonds for calcium binding (Zhang et al., 2018). To determine the contribution of these four residues in nvTRPM2 gating, we introduced the mutations to change the interaction force with calcium. The E893A mutant has little response to ADPR (Fig. 2a). Both E893D and E893Q mutants fail to be activated by ADPR (Figs. 2b and 2c), suggesting that this site is important for the nvTRPM2 channel gating.

Both Q896A mutation that shortened the side chain of glutamine and Q896E mutation that introduced negatively charged residue increased the current amplitude (Figs. 2e and 2f). In contrast, the Q896K mutant that introduced positively charged residue has no response to ADPR (Fig. 2g).

For N918, disrupting the polar solvation interaction by N918A mutation, or introducing a positive charge by N918K mutation, dramatically decreased the current amplitude (Figs. 2i and 2k). However, N918D, which added a negative charge without altering the side chain length, has a similar response to ADPR as wild-type (WT) nvTRPM2 (Fig. 2j), suggesting that side chain length instead of electronic force is critical for calcium-dependent channel gating.

Similar to E893, as another negatively charged residue within this calcium-binding site, D921 was mutated to alanine, lysine, or asparagine. All have a small response to ADPR (Figs. 2m–2p), suggesting that the negative charge of these residues mainly contributed to calcium-dependent channel gating.

These results demonstrated that these four residues which have the ability of calcium binding are related to nvTRPM2 channel activation.

3.3 Role of the four residues in S2–S3 loop of hTRPM2 on channel gating

Although the structure of hTRPM2 has been resolved recently (Wang et al., 2018), the calcium-binding site in the S2–S3 loop was not occupied by calcium. By performing the sequencing alignment of the S2–S3 loop between hTRPM2 and nvTRPM2, we found that the four residues in nvTRPM2 are very conserved across species (Fig. 3). The corresponding residues in hTRPM2 are E843, Q846, N869, and D872. Then, we addressed whether these conserved residues in hTRPM2 have a similar ability in regulating calcium-dependent channel gating.

Unlike nvTRPM2, the current of E843A mutant is similar to that of the hTRPM2 (Fig. 4a). E843D mutation, which slightly shortened the length of the side chain, has no function (Fig. 4b). This is the same as the E893D mutant. E843Q has a small current (Fig. 4c), which is also different from the E893Q mutant that has loss of function.

For Q846, the currents of both Q846A and Q846E mutants were obviously reduced compared to that of hTRPM2 (Figs. 4e and 4f). However, the Q846K mutant which introduced a positive charge showed a tiny current induced by ADPR (Fig. 4g). These data indicated that there are similar properties between Q896 and Q846 for TRPM2 channel gating.

For N869, N869A mutant, and positively charged N869K mutation have no response to ADPR (Figs. 4i and 4k). Nonetheless, similar to WT hTRPM2, the negatively charged N869D mutation was fully activated by ADPR (Fig. 4j). These data also indicated that there are similar properties between N918 and N869 for TRPM2 channel gating.

For D872, similar to D921 in nvTRPM2, D872A, D872K, and D872N mutants failed to be activated by ADPR (Figs. 4m–4p).

To exclude the possibility that the mutants with no current were due to their effects on surface expression of hTRPM2 channel, we performed a biotinylation assay for two representative mutants (E843D and D872K) of hTRPM2. Our result indicated that the E843D and D872K mutants can be delivered to the cell surface as well as WT hTRPM2 (Fig. 5), suggesting that these corresponding sites in the S2–S3 loop of hTRPM2 affect channel activation.

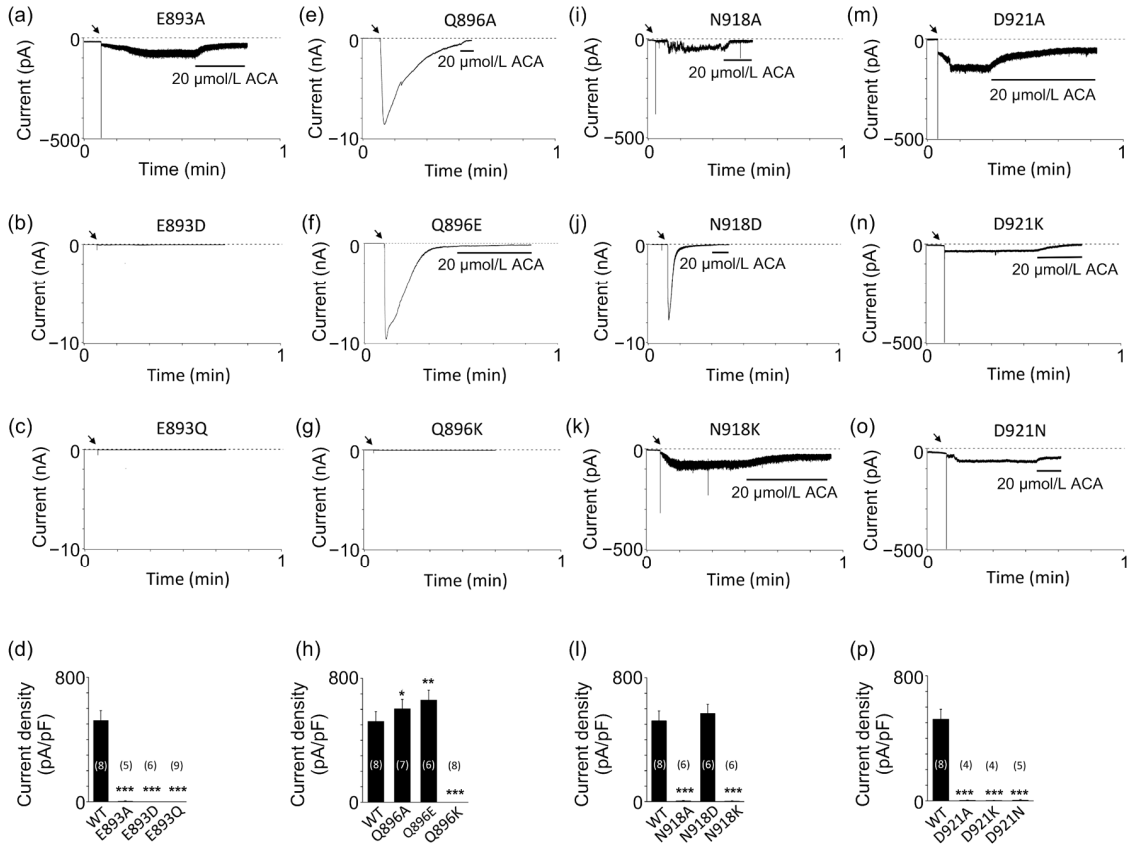

Fig. 2 Effect of mutants at four key residues within the identified calcium-binding site in S2–S3 loop of nvTRPM2 on channel gating

(a–c, e–g, i–k, m–o) Representative whole-cell recordings induced by 500 μmol/L adenosine diphosphate ribose (ADPR) with 10 mmol/L ethylene glycol tetraacetic acid (EGTA) at a holding membrane potential of −60 mV from HEK293T cells expressing E893A (a), E893D (b), E893Q (c), Q896A (e), Q896E (f), Q896K (g), N918A (i), N918D (j), N918K (k), D921A (m), D921K (n), and D921N (o) *Nematostella vectensis* transient receptor potential melastatin 2 (nvTRPM2) channels. The arrow in each panel indicates the time point at which whole-cell configuration was established. The black lines represent application of 20 μmol/L *N*-(pamylcinnamoyl) anthranilic acid (ACA). (d, h, l, p) Summary of the current density in a–c (d), e–g (h), i–k (l), m–o (p). Data are expressed as mean±standard error of the mean (SEM). The numbers of cells examined in each case are indicated in parentheses. * P<0.05, ** P<0.01, *** P<0.001, compared with wild type (WT)

Fig. 3 Sequencing alignment of S2–S3 loop between hTRPM2 and nvTRPM2

Arrows denote four residues discussed in the main text. Full conserved residues are marked in deep color

We noted that some mutants in hTRPM2 showed rapid inactivation just like nvTRPM2, such as Q846A (Fig. 4e), Q846E (Fig. 4f), and N869D (Fig. 4j). In addition, although nvTRPM2 has the characteristic of inactivation, mutations at the corresponding residues Q896 and N918 accelerated this process (that is Q896A (Fig. 2e), Q896E (Fig. 2f), and N918D (Fig. 2j)), suggesting that both glutamine and asparagine within the S2–S3 loop are involved in channel inactivation.

3.4 Regulation of the channel inactivation by glutamine within the calcium-binding site

To quantify the process of channel inactivation, we analyzed the percentage of the residual currents after inactivation from the peak currents (I_{remain}/I_{peak}). Since nvTRPM2 inactivation is much faster than hTRPM2 inactivation, we defined the percentage of the residual currents 40 or 10 s after the maximal

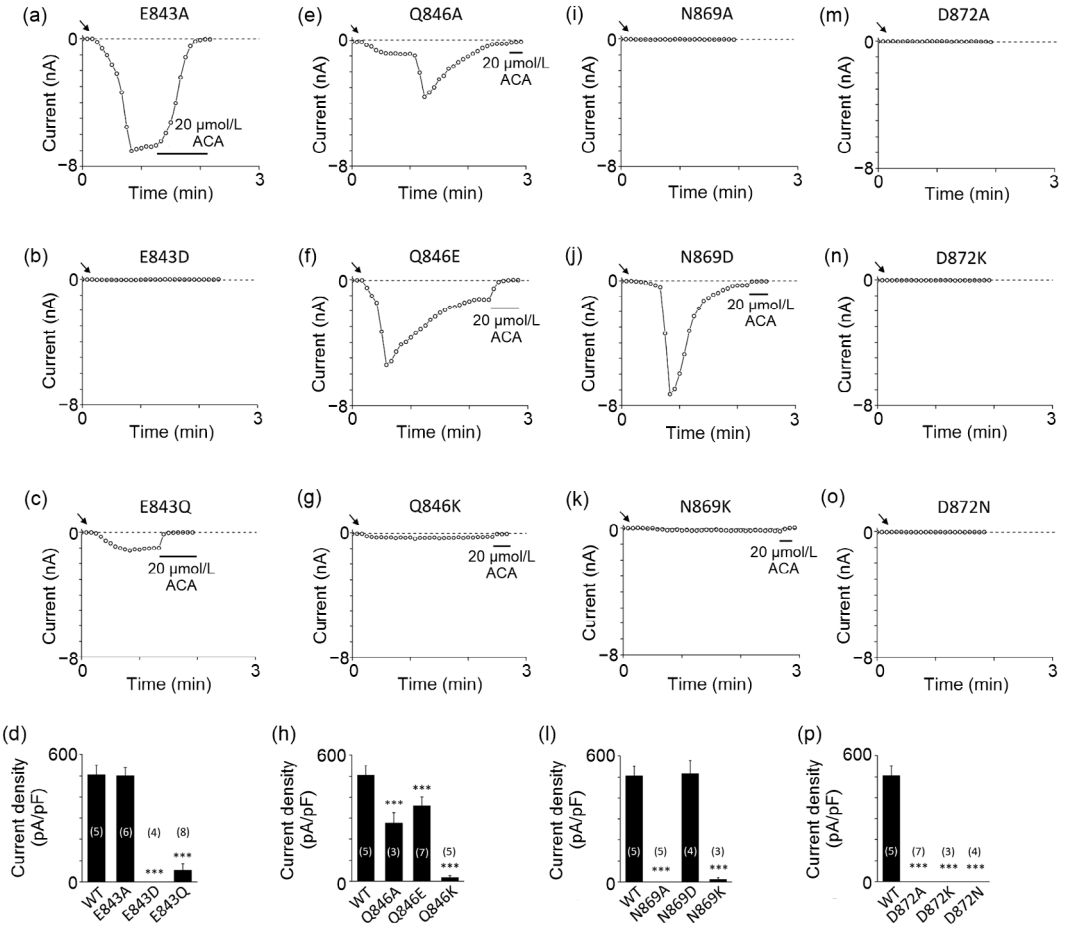

Fig. 4 Effect of mutants at four key residues within the identified calcium-binding site in S2–S3 loop of hTRPM2 on channel gating

(a–c, e–g, i–k, m–o) Representative whole-cell recordings induced by 500 μmol/L adenosine diphosphate ribose (ADPR) with 0.05 mmol/L ethylene glycol tetraacetic acid (EGTA) from HEK293T cells expressing E843A (a), E843D (b), E843Q (c), Q846A (e), Q846E (f), Q846K (g), N869A (i), N869D (j), N869K (k), D872A (m), D872K (n), and D872N (o) human transient receptor potential melastatin 2 (hTRPM2) channels. The arrow in each panel indicates the time point at which whole-cell configuration was established. The black lines represent application of 20 μmol/L *N*-(pamylcinnamoyl) anthranilic acid (ACA). (d, h, l, p) Summary of the current density in a–c (d), e–g (h), i–k (l), m–o (p). Data are expressed as mean±standard error of the mean (SEM). The numbers of cells examined in each case are indicated in parentheses. $^{***}P<0.001$, compared with wild type (WT)

currents from the peak currents ($I_{40\ s}/I_{peak}$ or $I_{10\ s}/I_{peak}$) as the inactivation rate of hTRPM2 or nvTRPM2.

The currents of WT nvTRPM2 declined completely after activation, and the residual currents were about 60% of the maximum amplitude 10 s after the peak (Figs. 6a, 6d, and 6e). Although Q896A and Q896E mutants resulted in complete channel inactivation (Fig. 6d), their inactivation rates were significantly smaller than that of WT nvTRPM2 (Fig. 6e).

Our previous studies showed that hTRPM2 current is stable within one minute after reaching the peak current (Yu et al., 2017; Luo et al., 2018), and both I_{remain}/I_{peak} and $I_{40\ s}/I_{peak}$ were more than 90% (Figs. 6f, 6i, and 6j). Unlike WT hTRPM2, both

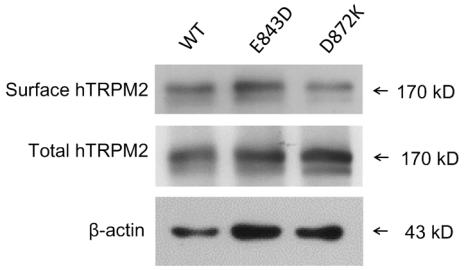

Fig. 5 Expression of E843D and D872K mutants from hTRPM2 on the surface of HEK293T cells

E843D and D872K were expressed on the surface of HEK293T cells. The top panel represents surface expression of human transient receptor potential melastatin 2 (hTRPM2), the middle panel represents total expression, and the bottom panel represents the expression of β-actin. Arrows denote the bands of wild-type (WT) hTRPM2 and the indicated mutants

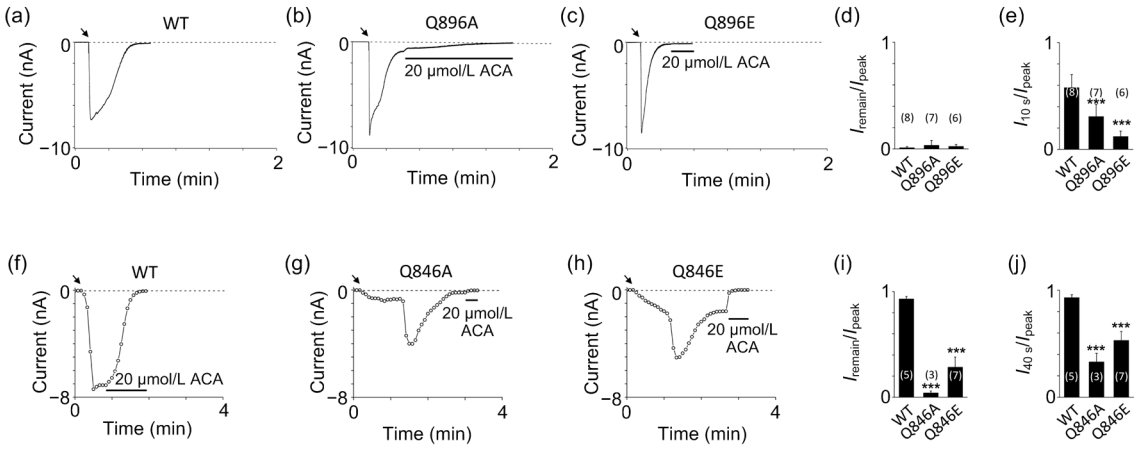

Fig. 6 Glutamine within calcium-binding site of S2–S3 loop facilitated channel inactivation in both nvTRPM2 and hTRPM2

(a–c) Representative whole-cell recordings induced by 500 μmol/L adenosine diphosphate ribose (ADPR) with 10 mmol/L ethylene glycol tetraacetic acid (EGTA) from HEK293T cells expressing wild type (WT) (a), Q896A (b), and Q896E (c) *Nematostella vectensis* transient receptor potential melastatin 2 (nvTRPM2) channels. (d, e) Summary of the inactivation degree, expressed as the percentage of the residual currents from the peak currents (d), and inactivation rate, expressed as the percentage of the residual currents 10 s after the maximal current amplitudes from the peak currents (e) of nvTRPM2. (f–h) Representative whole-cell recordings induced by 500 μmol/L ADPR with 0.05 mmol/L EGTA from HEK293T cells expressing WT (f), Q846A (g), and Q846E (h) human TRPM2 (hTRPM2) channels. (i, j) Summary of the inactivation degree, expressed as the percentage of the residual currents from the peak currents (i), and inactivation rate, expressed as the percentage of the residual currents 40 s after the maximal current amplitudes from the peak currents (j) of hTRPM2. The arrow in each panel indicates the time point at which whole-cell configuration was established. The black lines represent application of 20 μmol/L *N*-(pamylcinnamoyl) anthranilic acid (ACA). Data are expressed as mean±standard error of the mean (SEM). The numbers of cells examined in each case are indicated in parentheses. *** $P<0.001$, compared with WT

Q846A and Q846E mutants strongly induced channel inactivation. Compared to Q846E, Q846A resulted in complete inactivation, which decreased I_{remain}/I_{peak} to 0.041±0.018 (Fig. 6i) and $I_{40\ s}/I_{peak}$ to 0.330±0.080 (Fig. 6j).

3.5 Channel inactivation by asparagine within the calcium-binding site

By using the same statistics of channel inactivation rate as glutamine, our data indicated that N918D nvTRPM2 decreased the $I_{10\ s}/I_{peak}$ to 0.064±0.051 which was only about one-ninth of WT nvTRPM2 (Fig. 7d). Similarly, N869D mutant robustly decreased the residual currents and accelerated inactivation significantly (Figs. 7g and 7h).

4 Discussion

In this study, we determined that nvTRPM2 channel cannot be activated by calcium alone, and presents the fast activation that is similar to previous study (Kühn et al., 2015). Similar to nvTRPM2, the hTRPM2 channel also has a calcium-binding site in the S2–S3 loop, which is critical for activation or inactivation of hTRPM2. Moreover, our results identified that the negatively charged residues in the calcium-binding site are critical for channel activation, but glutamine and asparagine in the calcium-binding site are important for channel inactivation. These results indicated that the four key residues of the calcium-binding site in the S2–S3 loop mainly regulated the calcium-dependent channel gating process.

Previous studies have reported that calcium is essential to the hTRPM2 channel activation. For example, IQ-like motif of hTRPM2 that interacts with calmodulin is responsible for calcium-induced hTRPM2 activation (Du et al., 2009). Recently, our study identified a novel EF-loop in the N-terminus of hTRPM2, which is critical for hTRPM2 activated by calcium alone (Luo et al., 2018). In contrast, nvTRPM2 does not contain the IQ-like motif or EF-loop in the N-terminus, and this is consistent with nvTRPM2 failing to be activated by calcium alone in this study. These results further confirmed that the EF-loop and IQ-like motif in the N-terminus of hTRPM2 are responsible for calcium activation. In addition, a former study suggested that there is a

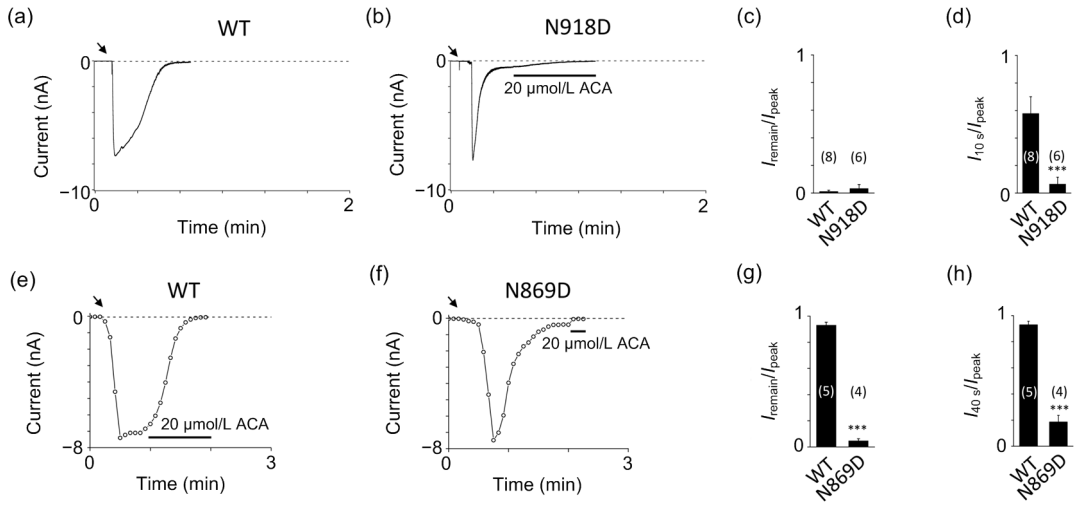

Fig. 7 Asparagine within calcium binding site of S2–S3 loop mutated to aspartate accelerated channel inactivation in both nvTRPM2 and hTRPM2

(a, b) Representative whole-cell recordings induced by 500 μmol/L adenosine diphosphate ribose (ADPR) with 10 mmol/L ethylene glycol tetraacetic acid (EGTA) from HEK293T cells expressing wild type (WT) (a) and N918D (b) *Nematostella vectensis* transient receptor potential melastatin 2 (nvTRPM2) channels. (c, d) Summary of the inactivation degree, expressed as the percentage of the residual currents from the peak currents (c), and inactivation rate, expressed as the percentage of the residual currents 10 s after the maximum current amplitudes from the peak currents (d) of nvTRPM2. (e, f) Representative whole-cell recordings induced by 500 μmol/L ADPR with 0.05 mmol/L EGTA from HEK293T cells expressing WT (e) and N869D (f) human TRPM2 (hTRPM2) channels. (g, h) Summary of the inactivation degree, expressed as the percentage of the residual currents from the peak currents (g), and inactivation rate, expressed as the percentage of the residual currents 40 s after the maximal current amplitudes from the peak currents (h) of hTRPM2. The arrow in each panel indicates the time point at which whole-cell configuration was established. The black lines represent application of 20 μmol/L *N*-(pamylcinnamoyl) anthranilic acid (ACA). Data are expressed as mean±standard error of the mean (SEM). The numbers of cells examined in each case are indicated in parentheses. *** $P<0.001$, compared with WT

calcium-binding site in the deep crevices near the pore of hTRPM2 intracellularly (Csanády and Törőcsik, 2009). Consistently, a recent study resolved the structure of nvTRPM2 by cryo-electron microscopy (cryo-EM), and clearly showed that there was a calcium-binding site in the S2–S3 loop (Zhang et al., 2018). Taken together, these results indicated that the calcium-dependent gating mechanisms of TRPM2 are very complex.

Sequence alignments show that the identified four residues are conserved among TRPM2 channels from different species. Except for hTRPM2 and nvTRPM2, it was reported recently that the corresponding residues (E857, Q860, N883, and D886) in zebrafish TRPM2 construct a calcium-binding site of the channel as well (Huang et al., 2018). Additionally, these sites are also found in TRPM4, TRPM5, and TRPM8, with the location near the pore, suggesting high conservation across the members of the melastatin subfamily of transient receptor potential proteins.

Our recordings of point mutants in four residues which formed the calcium-binding site of nvTRPM2 illustrate that mutations at E893 and D921 influence the channel currents strongly, which makes all the mutants difficult to be activated, demonstrating the importance of these two sites in calcium binding. In contrast, mutations at Q896 and N918 show milder influence on channel activation, with only Q896K, N918A, and N918K substantially altering the currents. Positively charged lysine substitutions at Q896 and N918 destroy calcium binding through electrostatic interaction, and the disabled function of N918A implies the importance of the side chain at this site.

Among the four residues, mutations at glutamine and asparagine have an effect on the inactivation process. For example, Q896A of nvTRPM2, which shortens the side chain of glutamine, accelerates channel inactivation by disturbing calcium binding, while Q846A of hTRPM2 induces channel inactivation. In addition, the excessive negative charge, which is introduced by Q896E and N918D for nvTRPM2 and Q846E and N869D for hTRPM2, also facilitates inactivation. Our data indicate that these four residues bind calcium through a rigid electrostatic equilibrium.

The negative charge from the mutation disturbs this balance, and this affects calcium binding and results in the channel inactivation. Our results indicated that although calcium binding in the S2–S3 loop of TRPM2 does not activate the channel directly, it seems to be an essential first step for channel opening, which induces conformational change and prepares TRPM2 to open. A similar function also exists in the calcium-binding site of TRPM4, which primes the channel to voltage-dependent opening (Autzen et al., 2018).

In summary, our results confirmed a calcium-binding site in the S2–S3 loop of both hTRPM2 and nvTRPM2, which plays a critical role for channel gating process. Instead of activating the channel directly, calcium binding to the S2–S3 loop primes TRPM2 to be ready for channel activation. Our study determined the effects of four residues in the S2–S3 loop on the TRPM2 channel gating, which deepened our understanding of the mechanism of the calcium-dependent TRPM2 channel gating process.

Contributors

Yu-huan LUO performed the experimental research. Yu-huan LUO and Wei YANG designed the experimentation, analyzed data, and wrote and edited the manuscript. Yu-huan LUO, Xia-fei YU, Cheng MA, and Fan YANG contributed to the data analysis and manuscript modification. All authors read and approved the final manuscript and, therefore, had full access to all the data in the study and take responsibility for the integrity and security of the data.

Compliance with ethics guidelines

Yu-huan LUO, Xia-fei YU, Cheng MA, Fan YANG, and Wei YANG declare that they have no conflict of interest.

This article does not contain any studies with human or animal subjects performed by any of the authors.

References

Autzen HE, Myasnikov AG, Campbell MG, et al., 2018. Structure of the human TRPM4 ion channel in a lipid nanodisc. *Science*, 359(6372):228-232. https://doi.org/10.1126/science.aar4510

Csanády L, Törőcsik B, 2009. Four Ca^{2+} ions activate TRPM2 channels by binding in deep crevices near the pore but intracellularly of the gate. *J Gen Physiol*, 133(2):189-203. https://doi.org/10.1085/jgp.200810109

Du JY, Xie J, Yue LX, 2009. Intracellular calcium activates TRPM2 and its alternative spliced isoforms. *Proc Natl Acad Sci USA*, 106(17):7239-7244. https://doi.org/10.1073/pnas.0811725106

Gao GF, Wang WW, Tadagavadi RK, et al., 2014. TRPM2 mediates ischemic kidney injury and oxidant stress through RAC1. *J Clin Invest*, 124(11):4989-5001. https://doi.org/10.1172/JCI76042

Hermosura MC, Cui AM, Go RCV, et al., 2008. Altered functional properties of a *TRPM2* variant in Guamanian ALS and PD. *Proc Natl Acad Sci USA*, 105(46):18029-18034. https://doi.org/10.1073/pnas.0808218105

Huang S, Turlova E, Li FY, et al., 2017. Transient receptor potential melastatin 2 channels (TRPM2) mediate neonatal hypoxic-ischemic brain injury in mice. *Exp Neurol*, 296:32-40. https://doi.org/10.1016/j.expneurol.2017.06.023

Huang YH, Winkler PA, Sun WN, et al., 2018. Architecture of the TRPM2 channel and its activation mechanism by ADP-ribose and calcium. *Nature*, 562(7725):145-149. https://doi.org/10.1038/s41586-018-0558-4

Jiang LH, Yang W, Zou J, et al., 2010. TRPM2 channel properties, functions and therapeutic potentials. *Expert Opin Ther Targets*, 14(9):973-988. https://doi.org/10.1517/14728222.2010.510135

Kheradpezhouh E, Ma LL, Morphett A, et al., 2014. TRPM2 channels mediate acetaminophen-induced liver damage. *Proc Natl Acad Sci USA*, 111(8):3176-3181. https://doi.org/10.1073/pnas.1322657111

Kühn F, Kühn C, Lückhoff A, 2015. Functional characterisation of a TRPM2 orthologue from the sea anemone *Nematostella vectensis* in human cells. *Sci Rep*, 5:8032. https://doi.org/10.1038/srep08032

Kühn F, Kühn C, Lückhoff A, 2017. Different principles of ADP-ribose-mediated activation and opposite roles of the NUDT9 homology domain in the TRPM2 orthologs of man and sea anemone. *Front Physiol*, 8:879. https://doi.org/10.3389/fphys.2017.00879

Lange I, Penner R, Fleig A, et al., 2008. Synergistic regulation of endogenous TRPM2 channels by adenine dinucleotides in primary human neutrophils. *Cell Calcium*, 44(6):604-615. https://doi.org/10.1016/j.ceca.2008.05.001

Li X, Jiang LH, 2018. Multiple molecular mechanisms form a positive feedback loop driving amyloid β42 peptide-induced neurotoxicity via activation of the TRPM2 channel in hippocampal neurons. *Cell Death Dis*, 9(2):195. https://doi.org/10.1038/s41419-018-0270-1

Luo YH, Yu XF, Ma C, et al., 2018. Identification of a novel EF-Loop in the N-terminus of TRPM2 channel involved in calcium sensitivity. *Front Pharmacol*, 9:581. https://doi.org/10.3389/fphar.2018.00581

Miller BA, Hoffman NE, Merali S, et al., 2014. TRPM2 channels protect against cardiac ischemia-reperfusion injury: role of mitochondria. *J Biol Chem*, 289(11):7615-7629. https://doi.org/10.1074/jbc.M113.533851

Nagamine K, Kudoh J, Minoshima S, et al., 1998. Molecular cloning of a novel putative Ca^{2+} channel protein (TRPC7)

highly expressed in brain. *Genomics*, 54(1):124-131. https://doi.org/10.1006/geno.1998.5551

Perraud AL, Fleig A, Dunn CA, et al., 2001. ADP-ribose gating of the calcium-permeable LTRPC2 channel revealed by Nudix motif homology. *Nature*, 411(6837): 595-599. https://doi.org/10.1038/35079100

Tóth B, Csanády L, 2010. Identification of direct and indirect effectors of the transient receptor potential melastatin 2 (TRPM2) cation channel. *J Biol Chem*, 285(39):30091-30102. https://doi.org/10.1074/jbc.M109.066464

Wang LF, Fu TM, Zhou YM, et al., 2018. Structures and gating mechanism of human TRPM2. *Science*, 362(6421): eaav4809. https://doi.org/10.1126/science.aav4809

Yang W, Zou J, Xia R, et al., 2010. State-dependent inhibition of TRPM2 channel by acidic pH. *J Biol Chem*, 285(40): 30411-30418. https://doi.org/10.1074/jbc.M110.139774

Yang W, Manna PT, Zou J, et al., 2011. Zinc inactivates melastatin transient receptor potential 2 channels via the outer pore. *J Biol Chem*, 286(27):23789-23798. https://doi.org/10.1074/jbc.M111.247478

Yonezawa R, Yamamoto S, Takenaka M, et al., 2016. TRPM2 channels in alveolar epithelial cells mediate bleomycin-induced lung inflammation. *Free Radic Biol Med*, 90: 101-113. https://doi.org/10.1016/j.freeradbiomed.2015.11.021

Yu PL, Xue XW, Zhang JM, et al., 2017. Identification of the ADPR binding pocket in the NUDT9 homology domain of TRPM2. *J Gen Physiol*, 149(2):219-235. https://doi.org/10.1085/jgp.201611675

Yu WY, Jiang LH, Zheng Y, et al., 2014. Inactivation of TRPM2 channels by extracellular divalent copper. *PLoS ONE*, 9(11):e112071. https://doi.org/10.1371/journal.pone.0112071

Zhang Z, Tóth B, Szollosi A, et al., 2018. Structure of a TRPM2 channel in complex with Ca^{2+} explains unique gating regulation. *Elife*, 7:e36409. https://doi.org/10.7554/eLife.36409

中文概要

题　目：S2–S3 loop 中钙离子结合位点对人类及海葵来源 TRPM2 通道门控过程的影响研究

目　的：揭示 S2–S3 loop 的钙离子结合位点对 M2 型瞬时受体电位通道（TRPM2）门控过程的影响。

创新点：首次探究了人类 TRPM2 通道（hTRPM2）和海葵 TRPM2 通道（nvTRPM2）S2–S3 loop 的钙离子结合位点内四个氨基酸残基不同突变对通道激活及失活过程的影响，明确了钙离子结合位点对通道门控的作用。

方　法：运用分子突变和电生理检测的方法，系统探究关键位点不同突变对 hTRPM2 和 nvTRPM2 激活及失活过程的影响，并采用生物素化及免疫印迹的方法，检测突变对通道表达上膜的影响。

结　论：（1）钙离子不能单独激活 nvTRPM2 通道；（2）hTRPM2 和 nvTRPM2 的四个关键氨基酸对钙离子依赖的门控调节作用类似；（3）在钙离子结合位点的四个关键氨基酸中，两个电负性氨基酸影响通道激活门控，两个电中性氨基酸影响通道失活门控。

关键词：M2 型瞬时受体电位通道（TRPM2）；钙离子结合位点；S2–S3 loop；通道激活；通道失活